Quantifying heterogeneous glacier dynamics in Lunana, Bhutan, using spatiotemporally high-resolution satellite imagery

Authors: \*Alex Hyde<sup>1</sup>, J. Rachel Carr<sup>1</sup>, Stuart Dunning<sup>1</sup>, Maximillian Van Wyk de Vries<sup>2,3</sup>

#### **Abstract**

The Lunana region in Bhutan, which hosts four large glacial lakes with significant hazard potential, has undergone rapid changes over the past decade. Using PlanetScope satellite scenes, we mapped ice velocities at monthly intervals from 2017 to 2023. We reveal that the disintegration of Thorthormi Glacier's terminus in 2022 coincided with year-on-year acceleration with mean surface velocities as high as  $448 \pm 10.0 \, \text{m a}^{-1}$  by 2021, and seasonal variability in surface velocity magnitude >144.6  $\pm 10.0 \, \text{m a}^{-1}$ . This acceleration is attributed to a reduction in basal drag as the terminus reached flotation, evidenced by the calving of tabular icebergs. While Bechung, Raphstreng, and Lugge exhibited a similar interannual velocity trend, the upper regions of Bechung and Raphstreng showed a higher seasonal range (31% and 19.9% from their mean) compared to Lugge (4.2%). In the upper regions we also find a decelerating velocity trend (3.5 – 20.6% over the 6 years), which is attributed to surface thinning and reducing driving stresses. We show that accelerating trends in velocity can be a precursor to higher rates of retreat and rapid lake expansion, demonstrating the importance of continuous monitoring of lake-terminating glacier ice velocities in the Himalaya.

#### 1. Introduction

Rates of glacier mass loss have increased in the Himalaya over the past 50 years: from 1974 to 2000 regional mass balance was estimated at -0.25 ±0.09 m.w.e. a<sup>-1</sup>, this increased to -0.39 ±0.12 m.w.e. a<sup>-1</sup> from 2000 to 2015 (King and others, 2019). These negative mass balance trends can be attributed to rising temperatures. The Himalaya have experienced faster temperature increases relative to surrounding low-lying regions, resulting in higher ablation rates that have not been offset by increased precipitation (Kraaijenbrink and others, 2017). Furthermore, these rates of change are not uniform. In the Eastern Himalaya, mass

This is an Open Access article, distributed under the terms of the Creative Commons Attribution licence (http://creativecommons.org/licenses/by/4.0), which permits unrestricted re- use, distribution and reproduction, provided the original article is properly cited.

<sup>\*</sup>Contact author: a.hyde2@newcastle.ac.uk

<sup>&</sup>lt;sup>1</sup>School of Geography, Politics and Sociology, Newcastle University, UK.

<sup>&</sup>lt;sup>2</sup>Department of Geography, University of Cambridge, Cambridge, UK

<sup>&</sup>lt;sup>3</sup>Department of Earth Science, University of Cambridge, Cambridge, UK

loss is nearly twice that of the central Himalaya and slightly higher than in Western Himalaya (Bolch and others, 2012; Kääb and others, 2012; Longwei and others, 2021; Zhang and others, 2023). The rate of mass balance change is also highest in Bhutan; mass balance has become increasingly negative, from -0.20 ±0.08 m.w.e. a<sup>-1</sup> (1974–2000), to -0.43 ±0.12 m.w.e. a<sup>-1</sup> (2000 to 2015), substantially lower than the Himalayan mean (King and others, 2019). Much of this variability can be explained by the increasing presence of proglacial lakes. 22% of glaciers in the Eastern Himalaya are lake-terminating, increasing from 14% in 2000, accounting for 29% of total mass loss (Komori, 2008; King and others, 2018; Zhang and others, 2023), with rates of lake growth projected to continue increasing in this region (Bajracharya and others, 2014; Maurer and others, 2019; Zhang and others, 2023).

Proglacial lake development results in accelerated mass loss through the initiation of calving-driven retreat and subaqueous melt (Carrivick and Tweed, 2013; Maurer and others, 2016; Liu and others, 2020; Watson and others, 2020). As the lake level increases, ice at the terminus can become buoyant, permitting calving, which can result in much larger volumes of mass loss than could occur through surface ablation alone (Kirkbride and others, 1993; Diolaiuti and others, 2006; Benn and others, 2007). Lake formation increases hydrostatic and subglacial water pressure, reducing bed friction and increasing basal sliding (Van der Veen, 2002; Carrivick and Tweed, 2013; Sutherland and others, 2020); resulting in flotation and a substantial reduction in basal friction, which in turn can promote acceleration and thinning (Wagner and others, 2016). This impact on glacial flow regime has resulted in half of lake-terminating glaciers in the region show an accelerating trend towards their termini, increasing the rate at which ice is transferred from accumulation to ablation zone. This contrasts with the broader trend of Himalayan glacier deceleration driven by thinning at lower elevations (Dehecq and others, 2019; Pronk and others, 2021).

However, the glacier response to lake formation and the subsequent rate of lake expansion in this region is highly variable, and the mechanisms driving this variability remain poorly understood. This is significant in the Eastern Himalaya, particularly in Bhutan, where glaciers not only provide water supply for hydropower and irrigation (Ministry of Economic Affairs, 2021), but also pose a risk to downstream communities from glacial hazards in the future, particularly from Glacial Lake Outburst Floods (GLOFs) (Komori and others, 2007). Bhutan alone has recorded 18 GLOF events since the 1950s, and has some of the highest risk basins globally (Watanabe and Rothacher, 1996; Iwata and others, 2002; Sakai, 2012; Fujita and others, 2012; Veettil and others, 2016; Rinzin and others, 2023; Taylor and others, 2023).

Satellite based remote sensing of ice velocities offers the most efficient path to the large scale monitoring of surface velocities. However, the monsoonal climate of the Bhutanese Himalaya, with cloud cover in the summer months makes the acquisition of satellite imagery challenging. Partial or full cloud coverage in the satellite images also limits the accuracy of feature tracking, and as a result, previous studies have omitted velocity measurements during the monsoon and therefore measurements have been seasonally restricted (Copland and others, 2011; Sato and others, 2022; Thongley and others, 2023). Furthermore, existing velocity products such as ITS\_LIVE, while effective for larger glaciers and ice caps, use feature tracking window sizes that are too big to accurately capture velocities for smaller mountain glaciers and lack the temporal resolution to measure short term changes in surface velocity (Gardner and others, 2018; Thongley and others, 2023; Scoffield and others, 2024).

The seasonality of ice dynamics in the region therefore remains poorly understood, particularly in the Lunana, Bhutan, where large scale changes to glacier area have been observed to occur at a seasonal-sub seasonal frequency. Thus, there is a pressing need to understand lake—glacier interactions to predict future glacier mass loss, lake formation and associated hazards. In this study we aim to: i) quantify large scale recent changes in ice velocity in Lunana, Bhutan at monthly scale from 2017 to 2023 using high resolution PlanetScope imagery, ii) examine the relationship between ice velocity, and the rapid calving retreat of Thorthormi that occurred over this study period, iii) investigate the relationship between changing ice dynamics and glacier thinning and the associated drivers behind the heterogeneous response of the four lake-terminating Lunana glaciers to lake development.

## 2. Study area

The study area comprises of the four large south facing lake-terminating glaciers in the Lunana region of Bhutan (Fig. 1). These glaciers originate from a high elevation icecap (6900 to 6100 m asl) forming part of Chomolhari Kang (28°9'59" N, 90°10'57" E). Bechung terminates at the lowest elevation (4406 m), followed by Raphstreng (4442 m), Thorthormi (4468 m), and Lugge (4518 m). Thorthormi was the largest by area in 2021, around 5.86 km², followed by Bechung (4.71 km²), Lugge (3.48 km²), and Raphstreng (1.85 km²). Both Bechung and Raphstreng are detached from the icecap, and receive much of their accumulation by avalanching. These two glaciers also have debris-covered terminus, with Thorthormi's terminus being around 90% debris-covered (2021), the ablation area of Lugge was around 60% clean ice in 2021. Precipitation is highest in the summer monsoon, with around 70% of annual rainfall occurring between June and September, with around 900 mm annual total (Suzuki and others, 2006). At Lugge, air temperatures have been shown to range from around -14 to 9°C (Suzuki and others, 2006).

Like elsewhere in the region, rates of glacier retreat and subsequent lake expansion for Bechung, Raphstreng, Thorthormi and Lugge have been heterogeneous. Lake development in the region began when Raphstreng Glacier transitioned from land to lake-terminating in 1967, retreating at 35 m a<sup>-1</sup>, accelerating to 60 m a<sup>-1</sup> from 1988, until the glacier became decoupled from the lake in 1998 (Ageta and others, 2000). In contrast, Lugge underwent continuous retreat since the late 1970s following proglacial lake development, at an average rate of 50 m a<sup>-1</sup>, with similar retreat rates at Bechung Glacier (Tsutaki and others, 2019). This is contrasted with the recent rapid retreat of Thorthormi Glacier, and the resultant expansion of a new large potentially dangerous lake that followed a period of apparent relative stability between 1990 and 2010. After the evolution of large lateral marginal lakes into a single proglacial lake in 2011, Thorthormi began an accelerated calving retreat, with an average annual retreat rate of 85 m a<sup>-1</sup> until 2014, increasing to 250 m a<sup>-1</sup> by 2020 (Sato and others, 2022), the next two years were followed by the break-up of the remaining terminus. Calving at this scale has not previously been observed in the Himalaya before (Sato and others, 2022), and may be indicative of dynamic thinning, a positive feedback processes that decreases a glacier's effective pressure altering the longitudinal stress

# Fig. 1 near here

balance, resulting in extensional flow and increased rates of calving (Benn and others, 2007; Carrivick and Tweed, 2013; King and others, 2018). Previous work in Lunana has revealed substantially higher velocities than the regional mean of 27.7 m a<sup>-1</sup> (Pronk and others, 2021), with velocities ranging from 160 to 280 m a<sup>-1</sup> recorded at Thorthormi within 2000 m of the Terminus from 2016 to 2017, and around 50 – 75 m a<sup>-1</sup> for the same region of Lugge (Sato and others, 2022).

## 3. Methodology

## 3.1 Imagery sources

We use the PlanetScope Dove constellation because of its daily/sub-daily return frequency. This enables us to maximise the number of clear summer days and hence the availability of imagery for feature tracking. This offers increased image availability during the monsoon relative to measurements made using platforms such as Sentinel-2 or Landsat 8, which have

# Fig 2 near hear

limited coverage between May and September (Fig. 2).

Alongside its short return frequency, PlanetScope's high spatial resolution (3m) compared to other commonly used platforms (Table 1), enables higher resolution velocity mapping.

Table 1. Near here

Orthorectified PlanetScope imagery between October 2016 and March 2024 was downloaded from Planet Explorer (planet.com/explorer/). Images with >20% identified as cloud were disregarded, leaving 526 images for the study period (Figure S1). To avoid interference from shadow motion, images were acquired at similar times: 90.1% were imaged between 03.30 and 04.50 UTC (09.30 and10.50 BTT). Initial testing by this study found that the default multiband PlanetScope images had the lowest stable ground uncertainty compared to velocimetry runs using individual Planet bands. Multiband image pairs also had consistently lower standard deviations and low percentage error compared to single band image pairs (Figure. S6). We therefore chose to use multiband composites comprised of either 4-band PS2 (PlanetScope Dove Classic) and PS2.SD (PlanetScope Dove-R) instruments) or 8-band PSB.SD (PlanetScope Super Dove) to calculate all velocimetry data. Multiband composites from PS2 and PS2.SD instruments return RGB and NIR bands, while PS2.SD instruments return RGB, Coastal Blue, Green i, Yellow, Red Edge, and NIR (Planet, 2024)

## 3.2 Processing

Imagery was clipped to include the full ice area for each glacier (Fig. 3). This also included off-ice areas of stable ground proximal to the glacier to which ice velocity was normalised in order to correct for any systematic georeferencing/orthorectification variability between image pairs (Van Wyk de Vries and Wickert, 2021). Stable ground regions were delineated following basin-wide Sentinel-2 velocimetry runs over an extended time series from 2017 to 2023, and defined as regions with detected ground motion <5 m a<sup>-1</sup>. Prior to use, all images were checked for any shifts on areas of ground where no movement is expected in the short term (e.g. ridge crests and gullies), if any movement was found, these images were removed. Any images with shading of ice areas were removed following manual examination of each time-series, as the changing position of shadows between images can be misinterpreted as ice motion (Lemmens, 1988). Only 37% of images had no detectable

Fig. 3 Near here

shadow, and the remainder had a mean shadow percentage of 1.53%.

# 3.3 Feature tracking

Ice velocity was determined using a technique known as Digital Image Correlation (DIC). This method measures the displacement of ice across a glacier's surface by comparing the position of identifiable features between two images taken at different times by tracking pixel brightness within a 'cross-correlation window' to give a value for the relative displacement

(Kääb and Vollmer, 2000; Fahnestock and others, 2016; Davison and others, 2020). Glacierwide values for displacement are converted into surface velocity by dividing the displacement in meters by the separation period between image pairs, this value is converted into annual velocity in m a<sup>-1</sup> (assuming 365 days in a year) (Kääb and Vollmer, 2000; Atkinson and Becker, 2020). DIC requires trackable features to be present. Cloud, snow cover and shadowing can reduce the number of trackable features such as crevasses and surface debris. Likewise, snowline retreat and shadow position change can be detected as 'ice motion' complicating measurements (Rosenau and others, 2015). To mitigate against these issues this study employs the feature tracking toolbox 'Glacial Image Velocimetry' (GIV) (Van Wyk de Vries and Wickert, 2021). The advantage of GIV, besides being accessible and simple to use, is the 'temporal oversampling' function which determines monthly velocities by tracking features between both consecutive and non-consecutive image pairs in order to produce a more accurate average velocity map for each month. This is particularly useful for Planet imagery that is sporadically spaced as it can account for the varying time difference between image pairs (Van Wyk de Vries and Wickert, 2021). This function also helps to average out the effect of poor or variable orthorectification between Planet images, resulting in substantial noise reduction.

The maximum interval between image pairs was varied between glaciers in order to compensate for differing flow regimes to prevent trackable features being lost on the fastest flowing ice (Table 2). Over increasing time, tracked features may move outside the cross-correlation window or simply change/break apart losing coherence and becoming untrackable. We therefore undertook a series of structured tests to establish the most appropriate max-min separation between image pairs for ice at different speeds. Maximum separations >100 days revealed increasing noise for ice velocities >280 m a<sup>-1</sup>. Maximum separations were therefore capped at 90 days to reduce feature loss and minimise the effect of changing seasonal illumination of features. This was reduced to 45 days for Thorthormi, due to the relative higher ice velocity for this glacier, and rapid deformation and breakup of features at the steep icefall resulting in increased loss of trackable features over time. The minimum period was maintained at 7 days for all glaciers in order to reduce the effect of inaccuracies in orthorectification relative to feature displacement.

The temporal oversampling value Table 2 near here defines the maximum number of image pairs that each available image is compared against; i.e. for a value of 2, image 1 is compared against image 2 as well as image 3. This value was maintained as high as computationally possible for each glacier, this ranged from between 10 and 15 image pairs (Table 2). A near-anisotropic orientation filter was applied to improve feature contrast, and images were further filtered through contrast-limited histogram equalisation, high-pass

filtering to reduce the effect of variable haze and lighting between image pairs (Van Wyk de Vries and Wickert, 2021; Agarwal and others, 2023).

GIV uses multiple passes to capture displacement over three gradually reducing window sizes. Our target output resolution was set to 40 m. This resulted in an initial window size of 160 m, halving with each iteration, resulting in an intermediate window size of 80 m. While initial tests were carried out using minimum window sizes (12m), this resulted in data loss for the fastest flowing ice. We found that a larger window was more effective in capturing the faster ice flow associated with Thorthormi Glacier, and icefall regions on Lugge, with 40 m offering an optimal balance between capturing ice flow, and maintaining a good image output resolution. This resolution is still significantly finer than other existing products thus maximising the benefit of the high-resolution Planet imagery. Velocity outputs were then filtered via signal-to-noise ratio <3 and a peak ratio <1.2, following Agarwal and others (2023). GIV excludes values greater than 1.5 standard deviations away from the monthly mean, ensuring that only values below this threshold are maintained (Van Wyk de Vries and Wickert, 2021). As GIV calculates monthly velocity averages, this is the frequency of velocity outputs used in this study.

## 3.4 Regions of interest

To compare ice velocity and surface elevation change over time, Bechung, Thorthormi and Lugge were divided into two regions of interest to separate the slower moving low gradient terminus ice, found below the lowest icefall of each glacier, and the faster flowing steeper 'upper' ice (Fig. 1) for analysis purposes. This was because ice velocity in these regions differs by an order of magnitude and the ice velocity response of ice to seasonal drivers also varies. Due to its smaller area and consistent gradient, Raphstreng is defined in one region. The lower region of Thorthormi was redefined for every month so that the lower boundary matched the location of the glacier terminus and excluded lake ice/icebergs to avoid spurious velocities. Ice velocities were extracted as the average value across each ROI for every month.

## Table 3. Near here

# 3.5 Estimating surface elevation change

We acquired two 2 m resolution digital elevation models (DEM) from the Pléiades Glacier Observatory - for October 2017 and November 2022 (Berthier and others, 2024). These DEMs were generated using the Semi-Global Matching approach (SGM), following the DEM pipeline developed by Berthier and others (2024) which employs the Ames Stereo Pipeline (Beyer and others, 2018). Both DEMs were coregistered to the Copernicus GLO-30 DEM

(European Space Agency, 2024). Surface elevation change (dH) for the four Lunana glaciers was estimated using z-based pixel differencing. Berthier and others (2024) measured an average uncertainty of 0.492 m for glacial area across the entire data set. We estimated an uncertainty of ±1.026 m by calculating the mean elevation difference across our stable ground area. The rates of thinning in the DEMs were compared with available directly measured data:

Measurements for surface elevation change between 2017 and 2022 for the terminus region of Lugge are comparable to DGPS measurements by Tsutaki and others (2019), although higher than Sato and others (2022) (Table 4).

#### Table 4 Near here

## 3.6 Uncertainty in surface flow velocity

Following error quantification approaches for ice velocities in previous work (Millan and others, 2019; Zhang and others, 2023), we used mean velocity across the stable-ground regions as an indirect reference for the relative uncertainty for each monthly velocity output. These regions are assumed to have close to zero displacement, relative to glacier ice, and provide a good reference for the relative uncertainty across the Region of Interest (ROI) being interrogated on each GIV run (Zhang and others, 2023). PlanetScope monthly ice velocities were then clipped to these areas and averaged for each month to give a value for stable ground.

In the absence of ground-based velocity data, we compared the GIV velocity results for PlanetScope against the 2017 to 2018 global ice velocity dataset from Millan and others (2022) (this data is available only for Lugge Glacier). While the Millan dataset may not be as accurate as other products, such as ITS\_LIVE (Gardner and others, 2018), the limited coverage of smaller glaciers in High Mountain Asia made ITS\_LIVE unsuitable for comparison in Lunana. To facilitate direct comparison, the PlanetScope annual velocity means were resampled to 50 m using bicubic interpolation, aligning with the resolution of the Millan product (Figure S2).

In addition, a secondary Sentinel-2 velocity dataset was generated using GIV. Sentinel-2 imagery was acquired via Planet Explorer (planet.com/explorer/). Band 4 was used as this band was typically less saturated than other bands over snowy ground (Kääb and others, 2016). The values for oversampling and maximum/minimum image separations were maintained as the same for each glacier as for the Planet imagery (Table 2). The process of filtering images for quality was also the same as for Planet imagery. Data from Thorthormi's upper region had a low signal-to-noise ratio, as snow and cloud cover hampered feature

tracking preventing comparison between Sentinel-2 and PlanetScope for this region. We compared velocities mean velocities across the upper and lower ROIs for Bechung and Lugge, the ROI for Raphstreng, and the lower region of Thorthormi (a lack of cloud free imagery and extensive snow cover resulted in the velocity data for the upper region of Thorthormi being unusable) (Figure. S3).

Following a similar approach to Sato and others (2022) we also conducted manual validation by measuring the horizontal displacement of 65 clearly identifiable crevasses and seracs between Sentinel-2 image pairs for 2019 (Figure S5). Measured displacement between image pairs was divided by days of image pair separation time and multiplied by 365. Manual measurements were compared directly with PlanetScope GIV outputs for the same period for Bechung, Thorthormi and Lugge. Raphstreng was excluded due to rapid loss of visible features between image pairs. Sentinel-2 was used, as its quality is well established and less prone to orthorectification issues making pairwise comparison more reliable, while the resolution is high enough for large features to be visible.

#### 4. Results

## 4.1 Spatial pattern of ice flow

There was a strong spatial dichotomy in flow regime between Thorthormi Glacier, Bechung, Raphstreng and Lugge (Fig. 4). At the latter three glaciers, velocities decelerated towards the terminus, with mean velocities in the terminus regions of Bechung and Lugge ROI (Fig. 1) ranging from 10 to 70 ±8.5 to 21.9 m a<sup>-1</sup>. In contrast, the low gradient terminus at Thorthormi exhibited downstream ice acceleration, with ice velocities ranging from 200 to 400 ±10.0 m a<sup>-1</sup>, an order of magnitude higher than its neighbouring glaciers. The steep upper regions of all glaciers were fast flowing, with Thorthormi and Lugge showing the fastest centreline velocities (200 to 420 ±10.0 to 8.5 m a<sup>-1</sup>), whereas Bechung and

# Fig 4 near here

Raphstreng were slightly slower (180 to 300 ±21.9 to 10.4 m a<sup>-1</sup>).

## 4.2 Temporal evolution of ice velocity

The seasonal pattern of velocity variability was relatively consistent between the study glaciers, but the magnitude of this change varied substantially (Fig. 5). Ice velocities for the terminus regions of the four glaciers typically peaked around spring/early-summer, while upper regions showed acceleration into early autumn, with all regions showing a yearly minimum in the winter. Lugge had an average seasonal ice velocity range of 35.5 ±8.5 m a<sup>-1</sup>

(63.2% of mean) for the lower region (Fig. 5), and a much lower 18.8 ±8.5 m a<sup>-1</sup> (8.3% of mean) for the upper region. In contrast, the lower region of Thorthormi had an average

## Fig 5 near here

seasonal range of 144.6 ±10.0 m a<sup>-1</sup> (44.7% of mean). This contrasted with the upper region of Thorthormi, which again had a lower seasonal variability (55 ±10.0 m a<sup>-1</sup>, 25.7% of mean), although substantially higher than Lugge's. Raphstreng, despite its small size, showed a large mean seasonal range (65.4 ±10.4 m a<sup>-1</sup>, 39.7% of mean), with ice velocities typically peaking around June-July, and reaching a seasonal low around March. The upper region of Bechung showed the highest seasonal variability, with a mean seasonal range of 66.5 ±21.9 m a<sup>-1</sup> (62% of mean). The velocity in the lower region of Bechung was also variable between months, however the relative change in velocity was comparable with the range in stable ground motion each month, so no clear pattern can be determined.

# 4.2.1 Temporal and spatial variability in seasonal ice velocity patterns from 2017 to 2023

Seasonal acceleration at Bechung was generally restricted to the upper region of the glacier, where ice acceleration occurred from spring (March to May) until autumn (September to November), followed by a rapid slowdown in winter (December to February) (Fig. 6a-c). The pattern of change for the lower region was not uniform and varied spatially across the terminus between all seasons. From 2017 to 2023 a diverging velocity trend emerged between the lower and upper regions. The lower region showed a mean increase in ice velocity of 7.5 ±21.9 m a<sup>-1</sup> (31.1% of mean), compared to a decrease of -9 ±21.9 m a<sup>-1</sup> (8.4% of mean) in mean ice velocity from 2017 to 2023 across the upper region.

Raphstreng showed a consistent annual pattern of summer acceleration and autumnal/winter deceleration (Fig. 6d-e). The lowest region of the glacier was the first to show a speed-up from winter to spring, by summer this acceleration was glacier wide, followed by a period of autumnal deceleration lasting into the winter. In the middle of the ROI there was a small region where acceleration occurred from Summer-Autumn and Autumn-Winter, with deceleration in the following two seasons. This area corresponded with a point where the glacier became partially detached and frequent seracs avalanches occurred over a steep bedrock band. While there was a slight negative trend in ice velocity over the study period (-5.7 ±10.4 m a<sup>-1</sup>, 3.5% of mean) there was little change in mean ice velocity from 2017 to 2023.

The lower region of Thorthormi exhibited continuous ice acceleration from winter into summer, with higher upstream ice velocities in early summer transferring ice downstream to the terminus (Fig. 6f-h). The seasonal acceleration in upstream ice velocity occurred later than at the terminus, with widespread ice acceleration occurring over the spring-summer period. This was followed by decelerating ice velocities in the highest regions (>6085 m a.s.l.) during autumn, although acceleration continued into the autumn 1.5 km downstream from the steep heavily crevassed icefalls (5200 m a.s.l.) down to the lower headwall (4630 m a.s.l.).

From 2017 to 2023, there was a divergent trend in ice velocities between the upper and lower regions of Thorthormi (Figs. 5, 6g-h). The upper region showed a decelerating trend, with a -53.7 ±10.0 m a<sup>-1</sup> (-23.7%) change in mean ice velocity from 2017 to 2023. In contrast, the terminus accelerated from 2017 to 2021, with maximum velocities increasing from 307 m a<sup>-1</sup>, peaking at 448.3 ±10.0 m a<sup>-1</sup> in June 2021. From 2017 to 2021 mean annual ice velocity in this region increased by 180.4 ±10.0 m a<sup>-1</sup> (74.8%), however by 2023 mean ice velocities in this region decreased by 104.5 ±10.0 m a<sup>-1</sup> from the 2021 peak (-24.8%).

Lugge experienced low magnitude seasonal acceleration relative to the other three glaciers. This peaked around late spring for all but the upper icefall (between 3.5 and 3.7 km from the terminus), with continued acceleration into the early autumn for the upper regions, but deceleration for the middle and lower parts of the glacier (Fig. 6j-k). Ice velocities increased slightly again in the autumn-winter transition particularly in the middle region of the glacier. The inter-annual velocity trend for Lugge revealed little overall change from 2017 to 2023, however, as with Bechung, there was a slight decelerating trend for the upper region ±8.5 m a<sup>-1</sup>, 5% of mean), in contrast to an accelerating trend for the lower terminus region (3.3 ±8.5

Fig. 6 Near here

m a<sup>-1</sup>, 5.9% of mean).

## 4.3 Surface elevation change from 2017 to 2022

Surface elevation change was greatest for the lower region of Lugge with a mean change of -24.1  $\pm 1.03$  m between 2017 and 2022 (-4.82  $\pm 0.17$  m  $a^{-1}$ ) (Fig. 7). The greatest change in surface elevation was seen at the transition between the lower region and the icefall of Thorthormi which showed a surface elevation change of more than -60 m (-12  $\pm 0.17$  m  $a^{-1}$ ). This contrasted with a mean change of -11.6  $\pm 1.03$  m (-2.32  $\pm 0.17$  m  $a^{-1}$ ) in the lower region. The lower region of Bechung also showed a substantial reduction in surface elevation, with a mean change of -14.7  $\pm 1.03$  m Raphstreng, at a slightly higher elevation also showed a

relatively consistent reduction in surface elevation with a mean difference of -9.4  $\pm$ 1.03 m. Surface elevation change was lower for the upper regions of all glaciers, with a -2.3  $\pm$ 1.03 m change for Lugge, and a -9.3  $\pm$ 1.03 m change for upper region of Thorthormi. The upper region of Thorthormi however, showed a sizeable variation in elevation in change (-68 -  $\pm$ 30  $\pm$ 1.03 m). The upper region of Bechung presents a change in mean surface elevation of -6.6  $\pm$ 1.03 m.

#### 5 Discussion

## 5.1 Heterogeneous glacier response to lake formation in Lunana

Our data showed that ice velocities for the four study glaciers are considerably higher than the Himalayan lake-terminating average of 18.8 m a<sup>-1</sup>, as well as the average for the Eastern Himalaya of 27.7 m a<sup>-1</sup> (Pronk and others, 2021). Relative to previous work we show that ice velocities for Thorthormi continued to increase, exceeding previous peak velocity measurements of 280 ±10.0 m a<sup>-1</sup>, while Lugge showed little change (Sato and others, 2022). We also reveal a contrasting pattern of velocity change over the study period between Thorthormi and the other three Lunana glaciers, Bechung, Raphstreng and Lugge. Specifically, we identified increasing variability in the seasonal ice velocities of the lower region of Thorthormi, coupled with an overall acceleration trend at low elevations between 2017 and 2022. The other three glaciers did not show an accelerating trend during the study period, nor do we find a consistent pattern of seasonal variability from year to year. Below we examine the differing dynamic behaviour of Thorthormi Glacier, despite similar climate forcing given the spatial proximity to the four Lunana glaciers.

The transition to much faster ice flow, exceeding 450 ±10.0 m a<sup>-1</sup> by 2021, followed a series of major break up events of the terminus. Between 2017 and 2018, the ice in the lower region detached from the valley sides and began calving of large tabular icebergs (Fig. 8). This may have de-buttressed the terminus, leading to a reduction in lateral and frontal shear stresses due to a loss in lateral confinement contributing to acceleration (Fig. 8c & d, Figure. S7) (Raymond, 1996; Schoof and others, 2017; Hill and others, 2020). In June 2019, a major breakup event coincided with a large landslide and GLOF event (Namgay, 2019; NCHM, 2020). This was followed by the re-advance of the lake calving terminus, with the winter lake freeze reducing ice motion in the lake, allowing ice to accumulate at the base of the icefall, allowing the lake calving terminus to extend to a size of 0.53 km² (Fig. 8e). This feature was highly fractured (Fig. 8f), and high ice velocities suggest that it may have been lightly grounded or floating, and was likely to be comprised of floating sections of ice that reformed into a semi-cohesive feature at the base of the glacier/lakes headwall. We find no comparable examples of such a rapid lake calving terminus formation in the existing

literature. The snout continued to extend down lake until the detachment of a large tabular iceberg in November 2021 (Fig. 8g). This was followed by little change over the following winter until 09/04/2022, when a large calving event led to the detachment of the remaining terminus ice (Fig. 8i); the white ice floating in the lake resulting from fracturing indicated the scale of this event. This detachment was followed by the continued breakup of the terminus ice, and evidence of calving of seracs from the glacier headwall was also observed (Fig. 8j).

The widespread flotation of a glacier terminus is rare in lacustrine environments because ice fronts typically become unstable upon reaching flotation (Warren and others, 2001; Carrivick and others, 2020). Consequently, observations of large, transitory floating terminus in laketerminating settings are uncommon. Where they have been documented, we find a number of cases with large tabular style calving, similar to that of Thorthormi. For instance, at the Mendenhall Glacier in Alaska, a floating terminus persisted for nearly two years before rapidly breaking into four large tabular icebergs during a period of accelerated ice flow (Boyce and others, 2007). Similarly, from 2012 to 2019, the San Quintín Glacier in Patagonia experienced a comparable retreat pattern. Bathymetry data at San Quintín Glacier revealed that this period of rapid calving coincided with the glacier retreating into an overdeepening, accompanied by a shift in surface velocities from deceleration to acceleration toward the terminus (Petlicki and others, 2023). This retreat was also associated with the formation of longitudinal fractures and the calving of elongated tabular icebergs (Podgórski and Petlicki, 2020). Rapid lacustrine calving has also been documented at Upsala Glacier, Patagonia, from a floating terminus, where high thinning rates drove periodic retreat (Naruse and Skvarca, 2000; Boyce and others, 2007; Moyer and others, 2016). Additionally, Holdsworth (1973) observed a lake-terminating outlet of the Barnes Ice Cap calving buoyant ice blocks fracturing within 50 meters of the terminus. The increasing frequency of large calving events at Thorthormi during the study period indicates that the terminus may have become progressively more buoyant, likely a result of progressive thinning of the terminus ice. This thinning would have also reduced the tensile and bending stresses of the terminus, resulting in higher strain rates, which would led to higher ice velocities and acceleration (Sugiyama and others, 2011; Tsutaki and others, 2019).

The increasingly high magnitude, high frequency seasonal changes in ice velocity we see for the lower region of Thorthormi between 2020 and 2023 indicate that the ice became increasingly sensitive to changing driving stresses as the terminus approached buoyancy. Ice that is close to its critical flotation thickness is more sensitive to thinning than well-grounded ice, thinning would drive increased buoyancy, lowering the overburden pressure and decreasing longitudinal stresses, resulting in acceleration (Warren and others, 2001; Kehrl and others, 2017; Carrivick and others, 2020; Pronk and others, 2021; Kellerer-

Pirklbauer and others, 2021). Importantly, we do not see an accelerating trend at the lower regions of Bechung and Lugge, or at Raphstreng in response to lake growth. This suggests that the terminus of these glaciers are grounded and not close to buoyancy (Boyce and others, 2007; Wagner and others, 2017). This suggests that the heterogeneous lake expansion may be primarily a response to substantially differing stress regimes at the terminus of Thorthormi and the other three glaciers.

## 5.2 Seasonal controls on ice dynamics in Lunana

While all four glaciers reveal a clear annual cycle in glacier speed, the timing of peak seasonal velocities for Bechung, Raphstreng and Lugge is also not coincident, and the seasonal velocity pattern for individual glaciers also varies between the years (Fig. 5). For example, ice velocities in the upper region of Bechung peak between September and November (Figs. 5a & 6a), where at Lugge this occurred between April and July (Figs 5d & 6i). Meanwhile, Raphstreng's ice velocities peaked in mid-summer (Figs. 5b & 6d)(June to August), and the upper region of Thorthormi undergoes two periods of annual acceleration, one in late spring/early summer (April to June), and another in autumn (September to November)(Figs. 5c & 6f). These variable trends in seasonal velocity change have been observed in the Himalaya generally (Zhang and others, 2023), and in the Nyainqêntanglha mountains in Tibet, with some glaciers showing velocities peaking in the winter, and others spring and summer (Zhang and others, 2020). We explore the relationship between glacier velocity in Lunana and its likely seasonal drivers, within the constraints of a lack of directly measured meteorological and hydrological data for Lunana.

## 5.2.1 Glacier velocity relationship with hydrological drivers

For all four glaciers, we observe a notable acceleration following the winter season (Figs. 5 & 6a,d,f,i). The initiation and magnitude of this acceleration are likely influenced by differences in each glacier's response to changing basal water pressure, the structure of their basal till, and the rate of subglacial drainage system closure due to creep (Hewitt, 2013; Vincent and Moreau, 2016; Armstrong and others, 2017). At both Raphstreng Glacier and the upper and lower regions of Thorthormi, we observe a strong acceleration signal during the early melt season, between early spring and early summer (Figs 5b,c & 6d,f). This is likely driven by increased surface melt overwhelming subglacial drainage systems that are adapted to winter conditions, such that as the input of meltwater increases, basal water pressures rises close to, or above the effective pressure, promoting enhanced basal sliding (Paterson, 1994; Sole and others, 2011).

At Raphstreng and in the upper region of Thorthormi, the initial peak in velocity during the spring/early summer is followed by a gradual deceleration (Figs 5b,c & 6d,f). This may be

due to the evolution of a more efficient, channelised subglacial drainage system in response to the increased water flow. As this system becomes more developed, it reduces basal water pressure and thus slows down glacier movement. Additionally, Raphstreng, Thorthormi, and Bechung all exhibit significant deceleration moving into the winter (Figs 5a,b,c & 6a,d,f), likely driven by the reduction in surface meltwater input and the viscous creep closure of subglacial water channels (Anderson and others, 2004; Hewitt, 2013).

## 5.2.2 Seasonal changes in driving stress

Seasonal acceleration may be driven in part by summer snowfall resulting in mass gain, and increased driving stresses (Jouberton and others, 2022; Zhang and others, 2023). The varying magnitude of the glacier response to a seasonal forcing is also a product of the relationship between the differing morphology of each glacier, such as varying overburden pressure (Zhang and others, 2023). For instance, Lugge Glacier exhibits low seasonal velocity variability (Fig 5), likely due to its location within a deep valley, resulting in higher resistive forces from the valley sides, with lateral resistive forces being shown to fluctuate less seasonally compared to basal resistive stress (Tripathi and others, 2023).

In contrast, Bechung, Raphstreng and Thorthormi lack similar buttressing along the glacier margins, receiving less resistance from the valley sides (Fig 5). As a result, the proportion of net drag from the margins is lower, making these glaciers more sensitive to changes in basal drag (Röthlisberger, 1972; Tripathi and others, 2023). This difference in resistive forces could explain the higher sensitivity of some of the Lunana glaciers to early season warming, while others that show a pattern of seasonal acceleration later in the melt season may be more sensitive to peaks in monsoonal precipitation during July and September (Suzuki and others, 2007; Naito and others, 2012).

Monsoonal precipitation also increases accumulation from avalanche activity, which, in turn, raises driving stress and ice velocity (Bhushan and others, 2024; Kneib and others, 2024). This could explain the late summer to early autumn peak in acceleration at the upper region of Bechung Glacier, which is primarily fed by avalanching (Fig 5a & 6a), as mass increases following high rates of monsoonal avalanching. Similarly, mass input from avalanches off the overhanging ice cap at Raphstreng Glacier could account for years in which high ice velocities persist into late autumn. The small region of acceleration identified on Raphstreng that occurred from summer into early winter (Fig. 6d), is an area associated with frequent serac collapses and avalanching, the detected increase in ice velocity most likely corresponds to an increase in avalanching during late summer to early winter.

At Thorthormi, our data suggests that the winter freezing of surface lake ice could play an important role in controlling seasonal ice velocities across the terminus. Calving rates were

much higher outside of the periods when the lake was frozen. In lake-terminating settings the freezing of the lake and ice mélange can impart sufficient back stresses to have stabilising effect on the calving front and lower region, contributing to a slowdown in ice loss as well as surface velocity (Geirsdóttir and others, 2008; Carrivick and others, 2020). The widespread presence of mélange at Thorthormi may have also been partially responsible for its higher magnitude seasonal cycles in ice velocity relative to the other Lunana glaciers, as mélange has been shown to be an important factor in marine terminating settings in strengthening frozen sea ice, resulting in much stronger back stresses (Amundson and others, 2010; Greene and others, 2018), the same may be true in a lake environment. Measurements of surface lake ice throughout the winter, as well as modelling of lake ice buttressing potential, in similar style to studies conducted at marine terminating glaciers (Greene and others, 2018; Parsons and others, 2024), would help to better constrain the importance of seasonal lake ice in controlling ice velocity in a high mountain setting.

We have compared several reanalysis datasets and found none to be representative of the few climate measurements available for Lunana. The nearest meteorological station with freely available data is in Gyatsa around 79 km away from Thorthormi glacier, this is therefore not utilised as it is also unlikely to be representative. Up to date meteorological data would be necessary to further constrain the environmental controls on ice dynamics in Lunana.

## 5.2.3 Velocity uncertainty

Ice velocities for Lugge, compared to the dataset produced by Millan and others (2022) were on average 11% (32.11 ±8.5 m a<sup>-1</sup>) faster for PlanetScope, however in the slower flowing terminus region, average ice velocities were 0.4% (-8.8 ±8.5 m a<sup>-1</sup>) slower for PlanetScope (Figure. S2). For our GIV generated Sentinel-2 dataset we found PlanetScope ice velocities to be 11% faster across all four glaciers. This ranged from 1.2% for the lower region of Bechung, to 21.2% for Thorthormi (Figure. S2). This compares to our manual feature tracking of Sentinel-2 image pairs where between Bechung, Thorthormi and Lugge, we found PlanetScope velocities to be on average 2.89 m a<sup>-1</sup> faster than measured velocities (r = 0.957)(Figure. S5).

Mean detected stable ground motion from 2017 to 2023 was lowest for Lugge (8.5 m a<sup>-1</sup>), followed by Thorthormi (10.0 m a<sup>-1</sup>) and Raphstreng (10.4 m a<sup>-1</sup>). The stable ground velocities at Bechung Glacier were notably higher (21.9 m a<sup>-1</sup>). These ranges are comparable with other similar studies (Millan and others, 2019; Tsutaki and others, 2019; Watson and others 2022; Tripathi and others, 2023; Zhang and others, 2023). Stable ground velocities for our Sentinel-2 dataset were higher than those for PlanetScope for Raphstreng

and Lugge (12.3 m  $a^{-1} - 8.3$  m  $a^{-1}$  respectively), and lower for Bechung and Thorthormi (8.2 m  $a^{-1} - 8.1$  m  $a^{-1}$  respectively)(Figure S4). The difference in stable ground velocities for Bechung for our PlanetScope data (11.5 m  $a^{-1}$  higher) compared to Sentinel-2 is indicative of the variable orthorectification quality with the PlanetScope product, and while images were filtered prior to registration, variable levels of distortion between image scenes would have resulted in higher values for stable ground motion. It may be that a lack of ground control points proximal to Bechung contributed to the ground surrounding this glacier having higher levels of distortion (Planet, 2019).

Ice velocities in this study consistently exceeded those derived from Sentinel-2, this likely a result of PlanetScope's shorter repeat imaging frequency, compared to Sentinel-2 allowing for improved tracking of the fastest moving features. These features are typically located at rapidly deforming icefalls and therefore remain coherent and trackable for shorter periods. Higher frequency imaging increases the probability of tracking these features before they move beyond the search window between repeat intervals. Using higher frequency imaging therefore results in a higher value for mean velocity.

Environmental factors are also important. Changing snow cover between image pairs can produce false matches and therefore erroneous velocity values, while slight changes to illumination conditions can generate differently shaped shadows having a similar effect, partially over variably featured stable ground (Mueting and Bookhagen, 2024). The rough, highly vegetated and boulder-strewn ground surrounding the study glaciers may have therefore contributed to the higher than average stable ground velocities for both the Sentinel-2 and PlanetScope datasets.

## 5.3 Surface elevation change

While the pattern of surface elevation change is relatively similar between all four glaciers in the basin, particularly in the upper regions, there are some notable disparities. The upper region of Thorthormi showed a considerable range in elevation change (-68 - +30  $\pm$ 1.03 m)(Fig. 7), much of this variability may be a result of changing positions of the large seracs present on the icefall over the sampling period. The large surface elevation change identified at the terminus headwall on Thorthormi (Fig. 7) may be indicative of a shift from compressive to extension flow in the terminus region, in part driving this thinning and movement of ice away from the headwall (Sato and others, 2022). We do not identify substantially higher thinning rates in the upper region of Thorthormi compared to Bechung, Raphstreng and Lugge, indicating the retreat of terminus at Thorthormi has not resulted in notable extensional flow and accelerated thinning relative to neighbouring glaciers.

As observed in other regions of High Mountain Asia and Bhutan, slower ice velocities have been attributed to reduced driving stresses resulting from thinning (Dehecq and others, 2019; Thongley and others, 2023). However, in Lunana, despite thinning across all four glaciers between 2017 and 2022 we did not find a net deceleration of glacier flow (Fig. 5-7). Although the lower regions of all glaciers show the most substantial thinning, we do not identify a large slowdown in ice velocity in these regions (Fig. 6c,h,k & 7). It is possible that ice velocities in the lower regions were sustained by increasing basal water flux and longer summer melt periods, driven by warmer mean annual air temperatures, offsetting the effect of reducing driving stresses (Vincent and Moreau, 2016; Goosse and others, 2018; Dehecq and others, 2019). If parts of Thorthormi's terminus were close to a critical flotation point, seasonal increases in thinning through surface melt across the terminus region may have been sufficient to result in portions of the terminus becoming ungrounded, with the associated reduction in basal drag contributing to the observed seasonal acceleration. Such a relationship between seasonal thinning and ice acceleration has been observed at Kangerlussuaq and Helheim glaciers in Greenland (Kehrl and others, 2017).

Regardless, despite the high ice velocities, mean rates of thinning across Thorthormi's terminus were not exceptionally high relative to the lower regions of its neighbouring glaciers (Fig. 7). The presence of very cold lake water, indirectly indicated by persistent icebergs and ice growlers, may have sustained the terminus by reducing rates of subaqueous melt and therefore thinning (Warren and others, 2001). At the Yakutat Glacier in Alaska, flotation was sustained over longer periods (months to years) when the water temperature was close to freezing (Trüssel and others, 2013). The importance of a debris mantle on the terminus will have also lowered thinning rates by insulating the ice, lowering rates of surface melt (Rowan and others, 2015), whereas Lugge had higher rates of thinning and at the terminus with a lower proportion of debris cover. Likewise, Bechung and Raphstreng both have significant debris coverage across their terminus and lower thinning rates, despite being at lower elevation than Lugge. The debris mantle may have delayed buoyant calving at Thorthormi as sediment cover increases the total mass of the ice column, resulting in a lower freeboard height and grounding at a greater water depth (Watson and others, 2020). Previous studies indicate that Thorthormi's lake may be unusually deep for the region (NCHM, 2019; Zhang and others, 2023). It is possible that this depth accommodated the development of an exceptionally thick terminus. This thickness may have been sufficient to support the tensile strength required to resist buoyant forces and longitudinal strain associated with buoyancy (Boyce and others, 2007). Constraints on lake bathymetry would provide a better understanding of the changing ice thickness over the study period and therefore terminus

conditions, with bed topography being necessary to quantify dynamic thinning and any potential retreat into an overdeepening.

The contrasting dynamic behaviour of Thorthormi Glacier compared to its neighbouring glaciers under similar environmental conditions, highlights the importance of understanding the localised controls on lake-terminating glacier dynamics. Unlike Bechung, Raphstreng, and Lugge glaciers, which show more stable or decelerating trends (Fig 5), Thorthormi's likely proximity to buoyancy made the terminus highly sensitive to short-term changes in driving stress, resulting in high magnitude changes in ice velocity. This highlights the role of subaqueous processes, such as thinning from melt and calving, which altered the glacier's stress regime, making it more sensitive to dynamic changes. While lake freezing in winter may have provided temporary stabilisation, the progressive thinning and floating of Thorthormi's terminus appear to have exacerbated its seasonal variability. In contrast, the grounded termini of the other Lunana glaciers exhibit less sensitivity to similar environmental changes. With lake-terminating glaciers becoming more numerous throughout the Himalaya (King and others, 2019), broader work should be undertaken to measure the changing pattern of ice velocity and surface elevation of different glaciers to lake formation in different regions of the Himalaya. This is crucial for predicting for assessing future risk from glacial hazards such as GLOFs, understanding water supply, as well as the wider scale implications of proglacial lake development on glacier dynamics throughout High Mountain Asia.

#### 6 Conclusions

This study provides a comprehensive analysis of surface ice velocity and dynamic changes across four lake-terminating glaciers in the Lunana region of Bhutan between 2017 and 2023. Our findings highlight the contrasting behaviours of Thorthormi compared to Bechung, Raphstreng, and Lugge, offering new insights into the role of proglacial lakes in glacier dynamics and retreat in the Himalaya.

We identified a substantial acceleration of Thorthormi Glacier, with annual peak velocities increasing from 307 ±10.0 m a<sup>-1</sup> in 2017 to 448 ±10.0 m a<sup>-1</sup> by 2021, driven by the breakup of its terminus and widespread flotation. We also observed an increasing magnitude in seasonal surface velocities variation for the lower region of Thorthormi over the study period, coinciding with thinning and calving of large tabular icebergs, suggesting widespread flotation of the terminus, and retreat driven by dynamic thinning. In contrast, the other three glaciers did not exhibit the same accelerating trend, though Bechung and Raphstreng showed considerable seasonal variability in ice velocities, particularly in their upper regions, while Lugge exhibited much lower variability without such strong seasonality.

The study revealed that glacier thinning in the upper regions of all four glaciers corresponded with a slight deceleration, yet the lower regions of Bechung and Lugge experienced a minor increase in velocity despite high thinning rates. An increased meltwater flux may be compensating for the loss of overburden pressure caused by thinning. However, the relationship between meltwater and ice velocity is also complex and strongly influenced by geometry and composition of the glacier bed and a glacier's stress regime. Our findings underscore that while proglacial lake expansion has a critical impact on glacier retreat, glacier behaviour can vary substantially, and is highly dependent on specific terminus conditions

This study is an important step in understanding how glacial outburst flood risk can increase over a short period of time, demonstrating the importance of routine surveying of lake-terminating glaciers that may be at risk of transitioning to a phase of rapid retreat. High resolution mapping of ice velocity can provide a useful indicator of a changing flow regime that could be indicative of acceleration preceding rapid retreat. Given the increasing prevalence of lake-terminating glaciers in the region, further work on the interactions between glacial dynamics, lake formation, and GLOF susceptibility are crucial for predicting the broader impacts of climate change on Himalayan glaciers and understanding the potential changes to outburst flood risk over the coming century.

**Supplementary material.** The Supplementary Material for this paper can be found at https://doi.org/xxxx

#### Acknowledgements

This research has been supported by the National Environmental Research Council (NERC) funded ONE Planet Doctoral Training Partnership (NE/S007512/1), hosted jointly by Newcastle and Northumbria universities. The authors would like to thank Etienne Berthier for kindly producing the two DEMs from our Pleiades imagery, used to calculate surface elevation change. We would also like to thank the reviewers and Scientific Editor for their helpful comments and contributions.

## **Conflict of interest**

The authors declare that the research was conducted in the absence of any commercial or financial relationships that could be construed as a potential conflict of interest.

#### References

- Agarwal V and 6 others (2023) Long-term analysis of glaciers and glacier lakes in the Central and Eastern Himalaya. *Science of the Total Environment*, 898, 165598. doi:10.1016/j.scitotenv.2023.165598
- Ageta Y and 5 others (2000) Expansion of glacier lakes in recent decades in the Bhutan Himalayas. *IAHS–AISH Publication*, 264
- Amundson JM, Fahnestock MA and Truffer M (2010) Ice mélange dynamics and implications for terminus stability, Jakobshavn Isbræ, Greenland. *Journal of Geophysical Research:* Earth Surface, 115(F1). doi:10.1029/2009JF001405
- Armstrong WH, Anderson RS and Fahnestock MA (2017) Spatial patterns of summer speedup on South-Central Alaska glaciers. *Geophysical Research Letters*, 44(18), 9379–9388. doi:10.1002/2017GL074370
- Atkinson D and Becker T (2020) A 117-line 2D digital image correlation code written in MATLAB. *Remote Sensing*, 12(18), 2906. doi:10.3390/rs12182906
- Benn DI, Warren CR and Mottram RH (2007) Calving processes and the dynamics of calving glaciers. *Earth-Science Reviews*, 82(3–4), 143–179. doi:10.1016/j.earscirev.2007.02.002
- Benn DI and 9 others (2012) Response of debris-covered glaciers in the Mount Everest region to recent warming, and implications for outburst flood hazards. *Earth-Science Reviews*, 114(1–2), 156–174. doi:10.1016/j.earscirev.2012.03.008
- Berthier E and 8 others (2024) The Pléiades Glacier Observatory: high-resolution digital elevation models and ortho-imagery to monitor glacier change. *The Cryosphere*, 18, 5551–5571. doi:10.5194/tc-18-5551-2024
- Beyer RA, Alexandrov O and McMichael S (2018) The Ames Stereo Pipeline: NASA's open-source software for deriving and processing terrain data. *Earth and Space Science*, 5, 537–548. doi:10.1029/2018EA000409
- Bhushan S, Shean D, Hu JM, Guillet G and Rounce DR (2024) Deriving seasonal and annual surface mass balance for debris-covered glaciers from flow-corrected satellite stereo DEM time series. *Journal of Glaciology*, 1–21. doi:10.1017/jog.2024.57
- Bolch T and 11 others (2012) The state and fate of Himalayan glaciers. *Science*, 336, 310–314. doi:10.1126/science.1215828
- Boyce ES, Motyka RJ and Truffer M (2007) Flotation and retreat of a lake-calving terminus, Mendenhall Glacier, Southeast Alaska, USA. *Journal of Glaciology*, 53(181), 211–224. doi:10.3189/172756507782202928
- Carrivick JL and Tweed FS (2013) Proglacial lakes: character, behaviour, and geological importance. Quaternary Science Reviews, 78, 34–52. doi:10.1016/j.quascirev.2013.07.028
- Carrivick JL, Tweed FS, Evans DJA, Roberts DH and Russell AJ (2020) Toward numerical modeling of interactions between ice-marginal proglacial lakes and glaciers. *Frontiers in Earth Science*, 8. doi:10.3389/feart.2020.577068
- Copland L and 5 others (2011) Expanded and recently increased glacier surging in the Karakoram. *Arctic, Antarctic, and Alpine Research*, 43(4), 503–516. doi:10.1657/1938-4246-43.4.503
- Cowton TR, Nienow PW, Sole AJ, Bartholomew ID, Mair DW and Slater DA (2018) Linear response of East Greenland's tidewater glaciers to ocean/atmosphere warming. *Proceedings of the National Academy of Sciences*, 115(31), 7907–7912. doi:10.1073/pnas.1801769115
- Cryosphere Services Division (2019) Reassessment of Potentially Dangerous Glacial Lakes in Bhutan. Thimphu: NCHM.
- Davison B and 6 others (2020) Subglacial drainage evolution modulates seasonal ice-flow variability of three tidewater glaciers in Southwest Greenland. *Journal of Geophysical Research: Earth Surface*, 125(9). doi:10.1029/2019JF005492

- Dehecq A and 9 others (2019) Twenty-first century glacier slowdown driven by mass loss in High Mountain Asia. *Nature Geoscience*, 12(1), 22–27. doi:10.1038/s41561-018-0271-9
- Diolaiuti G and 5 others (2006) Rates, processes and morphology of freshwater calving at Miage Glacier (Italian Alps). *Hydrological Processes*, 20(10), 2233–2244. doi:10.1002/hyp.6198
- European Space Agency (2023) Pléiades, Earth Online. Available at: https://earth.esa.int/eogateway/missions/pleiades (Accessed: 16 May 2024).
- European Space Agency (2023) Sentinel-2. Available at: <a href="https://www.esa.int/Applications/Observing\_the\_Earth/Copernicus/Sentinel-2">https://www.esa.int/Applications/Observing\_the\_Earth/Copernicus/Sentinel-2</a> (Accessed: 16 May 2024).
- European Space Agency (2023) SPOT 6, Earth Online. Available at: https://earth.esa.int/eogateway/missions/spot-6 (Accessed: 05 April 2025).
- European Space Agency (2023) SPOT 7, Earth Online. Available at: <a href="https://earth.esa.int/eogateway/missions/spot-7">https://earth.esa.int/eogateway/missions/spot-7</a> (Accessed: 05 April 2025).
- European Space Agency (2023) TerraSAR-X, Earth Online. Available at: <a href="https://earth.esa.int/eogateway/missions/terrasar-x-and-tandem-x">https://earth.esa.int/eogateway/missions/terrasar-x-and-tandem-x</a> (Accessed: 04 April 2025).
- European Space Agency (2024) Copernicus Global Digital Elevation Model. Distributed by OpenTopography. doi:10.5069/G9028PQB
- Fahnestock M and 5 others (2016) Rapid large-area mapping of ice flow using Landsat 8. Remote Sensing of Environment, 185, 84–94. doi:10.1016/j.rse.2015.11.023
- Fujita K and 6 others (2012) Outline of research project on glacial lake outburst floods in the Bhutan Himalayas. *Global Environmental Research*, 16, 3–12.
- Gardner AS and 6 others (2018) Increased West Antarctic and unchanged East Antarctic ice discharge over the last 7 years. *The Cryosphere*, 12(2), 521–547. doi:10.5194/tc-12-521-2018
- Geirsdóttir Á, Miller GH, Wattrus NJ, Björnsson H and Thors K (2008) Stabilization of glaciers terminating in closed water bodies: evidence and broader implications. *Geophysical Research Letters*, 35(17). doi:10.1029/2008GL034432
- Goosse H and 7 others (2018) Testing the consistency between changes in simulated climate and Alpine glacier length over the past millennium. *Climate of the Past*, 14(8), 1119–1133. doi:10.5194/cp-14-1119-2018
- Greene CA, Young DA, Gwyther DE, Galton-Fenzi BK and Blankenship DD (2018) Seasonal dynamics of Totten Ice Shelf controlled by sea-ice buttressing. *The Cryosphere*, 12(9), 2869–2882. doi:10.5194/tc-12-2869-2018
- Hewitt IJ (2013) Seasonal changes in ice-sheet motion due to meltwater lubrication. *Earth and Planetary Science Letters*, 371–372, 16–25. doi:10.1016/j.epsl.2013.04.022
- Hill EA, Gudmundsson GH, Carr JR, Stokes CR and King HM (2020) Twenty-first-century response of Petermann Glacier, northwest Greenland, to ice-shelf loss. *Journal of Glaciology*, 67(261), 147–157. doi:10.1017/jog.2020.97
- Holdsworth G (1973) Ice calving into the proglacial generator lake, Baffin Island, N.W.T, Canada. *Journal of Glaciology*, 12(65), 235–250. doi:10.3189/S0022143000032056
- Howat IM, Box JE, Ahn Y, Herrington A and McFadden EM (2010) Seasonal variability in the dynamics of marine-terminating outlet glaciers in Greenland. *Journal of Glaciology*, 56(198), 601–613. doi:10.3189/002214310793146232
- Iwata S, Narama C and Karma (2002) Three Holocene and late Pleistocene glacial stages inferred from moraines in the Lingshi and Thanza village areas, Bhutan. *Quaternary International*, 97–98, 69–78. doi:10.1016/S1040-6182(02)00052-6
- Jouberton A and 7 others (2022) Warming-induced monsoon precipitation phase change intensifies glacier mass loss in the southeastern Tibetan Plateau. *Proceedings of the National Academy of Sciences*, 119(37). doi:10.1073/pnas.2109796119
- Kääb A and Vollmer M (2000) Surface geometry, thickness changes and flow fields on creeping mountain permafrost: automatic extraction by digital image analysis.

- Permafrost and Periglacial Processes, 11(4), 315–326. doi:10.1002/1099-1530(200012)11:4<315::AID-PPP365>3.0.CO;2-J
- Kääb A, Berthier E, Nuth C, Gardelle J and Arnaud Y (2012) Contrasting patterns of early twenty-first-century glacier mass change in the Himalayas. *Nature*, 488(7412), 495–498. doi:10.1038/nature11324
- Kääb A and 5 others (2016) Glacier remote sensing using Sentinel-2. Part I: radiometric and geometric performance, and application to ice velocity. *Remote Sensing*, 8(7), 598. doi:10.3390/rs8070598
- Kehrl LM, Joughin I, Shean DE, Floricioiu D and Krieger L (2017) Seasonal and interannual variabilities in terminus position, glacier velocity, and surface elevation at Helheim and Kangerlussuaq glaciers from 2008 to 2016. *Journal of Geophysical Research: Earth Surface*, 122(9), 1635–1652. doi:10.1002/2016JF004133
- Kellerer-Pirklbauer A and 5 others (2021) Buoyant calving and ice-contact lake evolution at Pasterze Glacier (Austria) in the period 1998–2019. *The Cryosphere*, 15(3), 1237–1257. doi:10.5194/tc-15-1237-2021
- King O, Bhattacharya A, Bhambri R and Bolch T (2019) Glacial lakes exacerbate Himalayan glacier mass loss. *Scientific Reports*, 9, 18145. doi:10.1038/s41598-019-53733-x
- King O, Dehecq A, Quincey D and Carrivick J (2018) Contrasting geometric and dynamic evolution of lake- and land-terminating glaciers in the Central Himalaya. *Global and Planetary Change*, 167, 46–60. doi:10.1016/j.gloplacha.2018.05.006
- Kirkbride MP (1993) The temporal significance of transitions from melting to calving termini at glaciers in the central Southern Alps of New Zealand. *The Holocene*, 3(3), 232–240. doi:10.1177/095968369300300305
- Kneib M and 7 others (2024) Mapping and characterization of avalanches on mountain glaciers with Sentinel-1 satellite imagery. *The Cryosphere*, 18, 2809–2830. doi:10.5194/tc-18-2809-2024
- Komori J (2008) Recent expansions of glacial lakes in the Bhutan Himalayas. Quaternary International, 184(1), 177–186. doi:10.1016/j.quaint.2007.09.012.
- Lemmens M (1988) A survey on stereo matching techniques. *International Archives of Photogrammetry and Remote Sensing*, 27(B8), V11–V23.
- Liu Q and 6 others (2020) Interannual flow dynamics driven by frontal retreat of a laketerminating glacier in the Chinese Central Himalaya. *Earth and Planetary Science Letters*, 546, 116450. doi:10.1016/j.epsl.2020.116450
- Maurer JM, Rupper SB and Schaefer JM (2016) Quantifying ice loss in the eastern Himalayas since 1974 using declassified spy satellite imagery. *The Cryosphere*, 10, 2203–2215. doi:10.5194/tc-10-2203-2016
- Millan R, Mouginot J, Rabatel A and Morlighem M (2022) Ice velocity and thickness of the world's glaciers. *Nature Geoscience*, 15, 124–129. doi:10.1038/s41561-021-00885-z
- Millan R and 6 others (2019) Mapping surface flow velocity of glaciers at regional scale using a multiple-sensors approach. *Remote Sensing*, 11(21), 2498. doi:10.3390/rs11212498
- Ministry of Economic Affairs (2021) Bhutan Sustainable Hydropower Development Policy 2021. Royal Government of Bhutan, Thimphu.
- Minowa M, Schaefer M and Skvarca P (2023) Effects of topography on dynamics and mass loss of lake-terminating glaciers in southern Patagonia. *Journal of Glaciology*, 1–18. doi:10.1017/jog.2023.42
- Moyer AN, Moore RD and Koppes MN (2016) Streamflow response to the rapid retreat of a lake-calving glacier. *Hydrological Processes*, 30, 3650–3665.
- Mueting A and Bookhagen B (2024) Tracking slow-moving landslides with PlanetScope data: new perspectives on the satellite's perspective. *Earth Surface Dynamics*, 12, 1121–1143. doi:10.5194/esurf-12-1121-2024
- Naito N and 7 others (2012) Recent glacier shrinkages in the Lunana region, Bhutan Himalayas. *Global Environmental Research*, 16, 13–22.
- National Centre for Hydrology and Meteorology (2020) Detailed Assessment Report on GLOF Hazard from Thorthormi Glacial Lake and Associated Glaciers (Field season: September–October 2019). Thimphu.

- National Centre for Hydrology and Meteorology and Namgay W (2019) *Outburst of the Thorthormi Subsidiary Lake II on June 20, 2019.* Thimphu.
- Nie Y and 5 others (2018) An inventory of historical glacial lake outburst floods in the Himalayas based on remote sensing observations and geomorphological analysis. *Geomorphology*, 308, 91–106. doi:10.1016/j.geomorph.2018.02.002
- Paterson WSB (1994) The Physics of Glaciers. 3rd edn. Oxford: Pergamon.
- Parsons R, Sun S and Gudmundsson H (2024) Quantifying the buttressing contribution of sea ice to Crane Glacier. *EGUsphere* [Preprint]. doi:10.5194/egusphere-egu24-12813
- Paul F and 9 others (2022) Three different glacier surges at a spot: what satellites observe and what not. *The Cryosphere*, 16, 2505–2526. doi:10.5194/tc-16-2505-2022
- Planet Labs (2019) Planet Imagery Product Specifications. Available at: <a href="https://assets.planet.com/docs/combined-imagery-product-spec-april-2019.pdf">https://assets.planet.com/docs/combined-imagery-product-spec-april-2019.pdf</a> (Accessed: 04 April 2025).
- Planet Labs (2024) PlanetScope sensor data. Available at: <a href="https://developers.planet.com/docs/apis/data/sensors/">https://developers.planet.com/docs/apis/data/sensors/</a> (Accessed: 30 November 2024).
- Planet Labs (2024) RapidEye. Available at: https://developers.planet.com/docs/data/rapideye/ (Accessed: 16 May 2023).
- Pronk JB, Bolch T, King O, Wouters B and Benn DI (2021) Contrasting surface velocities between lake- and land-terminating glaciers in the Himalayan region. *The Cryosphere*, 15(12), 5577–5599. doi:10.5194/tc-15-5577-2021
- Raymond C (1996) Shear margins in glaciers and ice sheets. *Journal of Glaciology*, 42(140), 90–102. doi:10.3189/S0022143000030550
- Rinzin S, Zhang G and Wangchuk S (2021) Glacial-lake area change and potential outburst-flood hazard assessment in the Bhutan Himalaya. *Frontiers in Earth Science*, 9. doi:10.3389/feart.2021.775195
- Rinzin S and 7 others (2023) GLOF hazard, exposure, vulnerability, and risk assessment of potentially dangerous glacial lakes in the Bhutan Himalaya. *Journal of Hydrology*, 619. doi:10.1016/j.jhydrol.2023.129311
- Robel AA (2017) Thinning sea ice weakens buttressing force of iceberg mélange and promotes calving. *Nature Communications*, 8(1). doi:10.1038/ncomms14596
- Robertson CM, Brook MS, Holt KA, Fuller IC and Benn DI (2013) Calving retreat and proglacial lake growth at Hooker Glacier, Southern Alps, New Zealand. *New Zealand Geographer*, 69(1), 14–25. doi:10.1111/nzg.12001
- Rosenau R, Scheinert M and Dietrich R (2015) A processing system to monitor Greenland outlet-glacier velocity variations at decadal and seasonal time scales utilizing Landsat imagery. *Remote Sensing of Environment*, 169, 1–19. doi:10.1016/j.rse.2015.07.012
- Röthlisberger H (1972) Water pressure in intra- and subglacial channels. *Journal of Glaciology*, 11(62), 177–203. doi:10.1017/S0022143000022188
- Rowan AV, Egholm DL, Quincey DJ and Glasser NF (2015) Modelling the feedbacks between mass balance, ice flow and debris transport to predict the response to climate change of debris-covered glaciers in the Himalaya. *Earth and Planetary Science Letters*, 430, 427–438. doi:10.1016/j.epsl.2015.09.004
- Ruiz L, Berthier E, Masiokas M, Pitte P and Villalba R (2015) First surface velocity maps for glaciers of Monte Tronador, North Patagonian Andes, derived from sequential Pléiades satellite images. *Journal of Glaciology*, 61(229), 908–922. doi:10.3189/2015JoG14J134
- Sakai A (2012) Glacial lakes in the Himalayas: a review on formation and expansion processes. *Global Environmental Research*, 16, 23-30.
- Sato Y, Fujita K, Inoue H, Sakai A and Karma (2022) Land- to lake-terminating transition triggers dynamic thinning of a Bhutanese glacier. *The Cryosphere*, 16(6), 2643–2654. doi:10.5194/tc-16-2643-2022
- Schaffer N, Copland L and Zdanowicz C (2017) Ice-velocity changes on Penny Ice Cap, Baffin Island, since the 1950s. *Journal of Glaciology*, 63(240), 716–730. doi:10.1017/jog.2017.40

- Schoof C, Davis AD and Popa TV (2017) Boundary-layer models for calving marine outlet glaciers. *The Cryosphere*, 11(5), 2283–2303. doi:10.5194/tc-11-2283-2017
- Scoffield AC and 5 others (2024) Sub-regional variability in the influence of ice-contact lakes on Himalayan glaciers. *Journal of Glaciology*, 1–11. doi:10.1017/jog.2024.9
- Shean DE and 5 others (2020) A systematic, regional assessment of High Mountain Asia glacier mass balance. *Frontiers in Earth Science*, 7, 363. doi:10.3389/feart.2019.00363
- Shi Y and 8 others (2024) Glacial lakes control ice flow: new insights from satellite SAR PO-SBAS observations in Duiya Glacier, southern Tibetan Plateau. *International Journal of Digital Earth*, 17(1), 2365964. doi:10.1080/17538947.2024.2365964
- Sole AJ and 6 others (2011) Seasonal speedup of a Greenland marine-terminating outlet glacier forced by surface melt-induced changes in subglacial hydrology. *Journal of Geophysical Research*, 116(F3). doi:10.1029/2010JF001948
- Sugiyama S and 7 others (2021) Subglacial discharge controls seasonal variations in the thermal structure of a glacial lake in Patagonia. *Nature Communications*, 12(1). doi:10.1038/s41467-021-26578-0
- Sugiyama S and 7 others (2011) Ice speed of a calving glacier modulated by small fluctuations in basal water pressure. *Nature Geoscience*, 4, 597–600. doi:10.1038/ngeo1218
- Sutherland JL and 5 others (2020) Proglacial lakes control glacier geometry and behavior during recession. *Geophysical Research Letters*, 47, e2020GL088865. doi:10.1029/2020GL088865
- Suzuki R and 5 others (2007) Meteorological observations during 2002–2004 in the Lunana region, Bhutan Himalayas. *Bulletin of Glaciological Research*, 24, 71–78.
- Taylor C, Robinson TR, Dunning S and Westoby M (2023) Glacial lake outburst floods threaten millions globally. *Nature Communications*, 14, 487. doi:10.1038/s41467-023-36033-x
- Thongley PK and 5 others (2023) Estimation of glacier dynamics of the major glaciers of Bhutan using geospatial techniques. *Journal of Water and Climate Change*, 14(8), 2825–2841. doi:10.2166/wcc.2023.158
- Tripathi N, Singh SK, Rathore BP, Oza SR and Bahuguna IM (2023) Topographical and morphological variability explicates the regional heterogeneity in glacier surface ice velocity across Karakoram–Himalaya. *Remote Sensing Applications: Society and Environment*, 29, 100892. doi:10.1016/j.rsase.2022.100892
- Trüssel BL, Motyka RJ, Truffer M and Larsen CF (2013) Rapid thinning of lake-calving Yakutat Glacier and the collapse of the Yakutat Icefield, Southeast Alaska, USA. *Journal of Glaciology*, 59(213), 149–161. doi:10.3189/2013JoG12J081
- Tsutaki S and 6 others (2019) Contrasting thinning patterns between lake- and land-terminating glaciers in the Bhutanese Himalaya. *The Cryosphere*, 13(10), 2733–2750. doi:10.5194/tc-13-2733-2019
- U.S. Geological Survey (2023) Landsat 7. Available at: <a href="https://www.usgs.gov/landsat-missions/landsat-7">https://www.usgs.gov/landsat-missions/landsat-7</a> (Accessed: 16 May 2023).
- U.S. Geological Survey (2023) Landsat 8. Available at: <a href="https://www.usgs.gov/landsat-missions/landsat-8">https://www.usgs.gov/landsat-missions/landsat-8</a> (Accessed: 16 May 2023).
- Van der Veen CJ. (2002) Calving glaciers. *Progress in Physical Geography*, 26, 96–122. doi:10.1191/0309133302pp327ra
- Van Wyk de Vries M and Wickert AD (2021) Glacier Image Velocimetry: an open-source toolbox for easy and rapid calculation of high-resolution glacier velocity fields. *The Cryosphere*, 15(4), 2115–2132. doi:10.5194/tc-15-2115-2021
- Veettil BK and 5 others (2016) Glacier changes and related glacial-lake expansion in the Bhutan Himalaya, 1990–2010. *Regional Environmental Change*, 16, 1267–1278. doi:10.1007/s10113-015-0853-7
- Veh G, Garcia-Castellano D and Korup O (2020) Evolving hazards from Himalayan glacial-lake outburst floods. *EGU* 2020 [Preprint]. doi:10.5194/egusphere-egu2020-3486

- Vincent C and Moreau L (2016) Sliding-velocity fluctuations and subglacial hydrology over the last two decades on Argentière Glacier, Mont Blanc area. *Journal of Glaciology*, 62(235), 805–815. doi:10.1017/jog.2016.35
- Wagner TJ, Payne AJ, Cornford SL and Moon T (2016) On the role of buoyant flexure in glacier calving. *Geophysical Research Letters*, 43(1), 232-240. doi:10.1002/2015GL067247
- Walter JI and 6 others (2012) Oceanic mechanical forcing of a marine-terminating Greenland glacier. *Annals of Glaciology*, 53(60), 181–192. doi:10.3189/2012AoG60A083
- Warren C, Benn D, Winchester V and Harrison S (2001) Buoyancy-driven lacustrine calving, Glaciar Nef, Chilean Patagonia. *Journal of Glaciology*, 47(156), 135–146. doi:10.3189/172756501781832403
- Watanabe T and Rothacher D (1996) The 1994 Lugge Tsho glacial-lake outburst flood, Bhutan Himalaya. *Mountain Research and Development*, 16(1), 77–81. doi:10.2307/3673897
- Watson CS and 5 others (2020) Mass loss from calving in Himalayan proglacial lakes. Frontiers in Earth Science, 7. doi:10.3389/feart.2019.00342
- Xiang L and 5 others (2021) Glacier mass balance in High Mountain Asia inferred from a GRACE release-6 gravity solution for the period 2002–2016. *Journal of Arid Land*, 13, 224–238. doi:10.1007/s40333-021-0094-1
- Zhang G and 9 others (2023) Underestimated mass loss from lake-terminating glaciers in the Greater Himalaya. *Nature Geoscience*, 16, 333–338. doi:10.1038/s41561-023-01150-1
- Zhang J, Jia L, Menenti M and Ren S (2021) Interannual and seasonal variability of glacier surface velocity in the Parlung Zangbo Basin, Tibetan Plateau. *Remote Sensing*, 13(1), 80. doi:10.3390/rs13010080
- Zhang Z, Xu Y, Liu S, Ding J and Zhao J (2023) Seasonal variations in glacier velocity in the High Mountain Asia region during 2015–2020. *Journal of Arid Land*, 15(6), 637–648. doi:10.1007/s40333-023-0016-5

## Figure captions

**Fig. 1.** Lunana region in the context of Bhutan (a). Lunana overview, including the four study glaciers; Bechung, Raphstreng, Thorthormi, and Lugge (b). Red and blue polygons indicating lower and upper areas of interest for each glacier. (Basemap: PlanetScope. 2021).

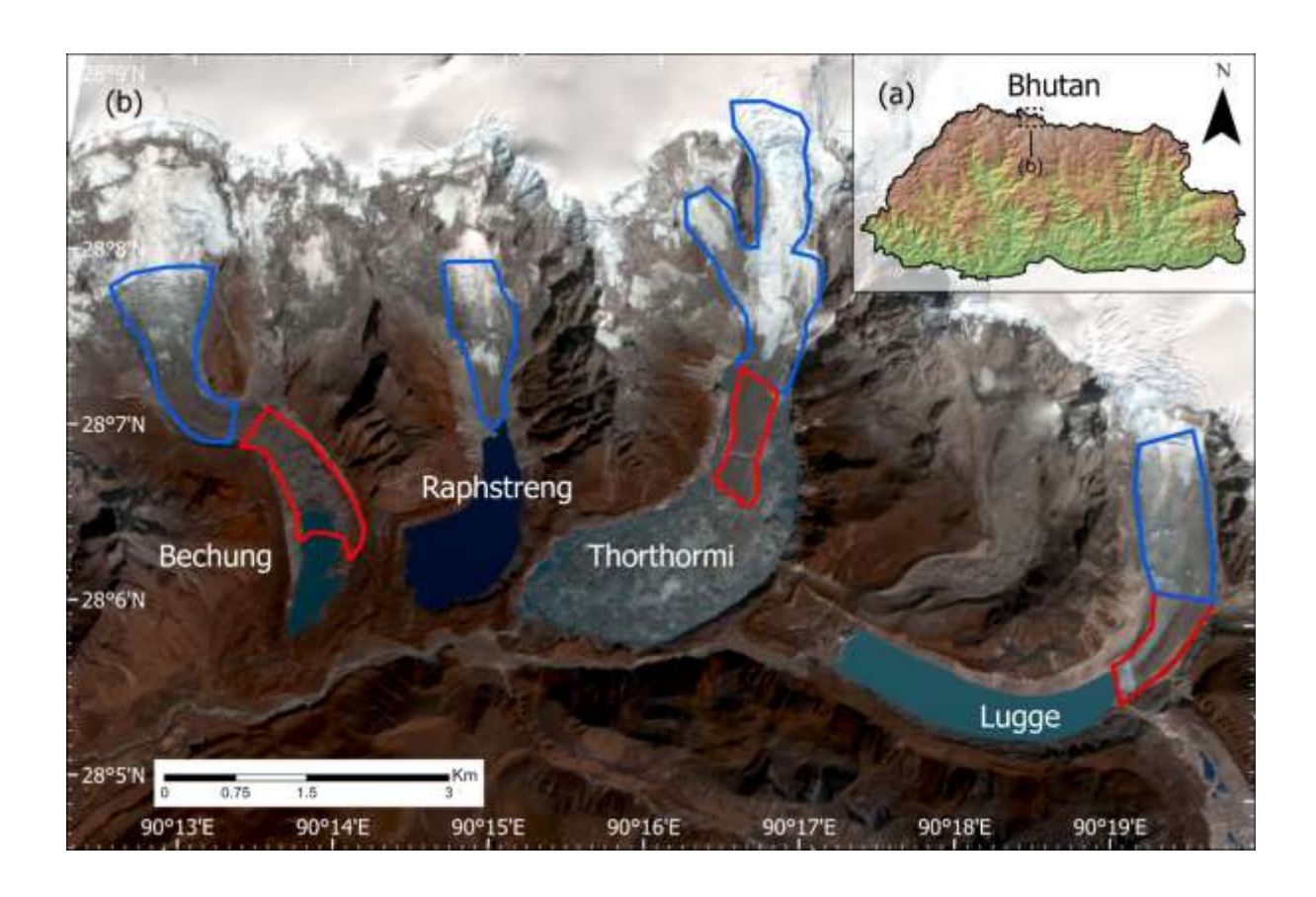


**Fig. 2.** Total availability of cloud-free (>80% of pixels) PlanetScope *Dove* imagery between 2017 and 2023 for Lunana. Compared with Sentinel-2 and Landsat 8 for the same period.

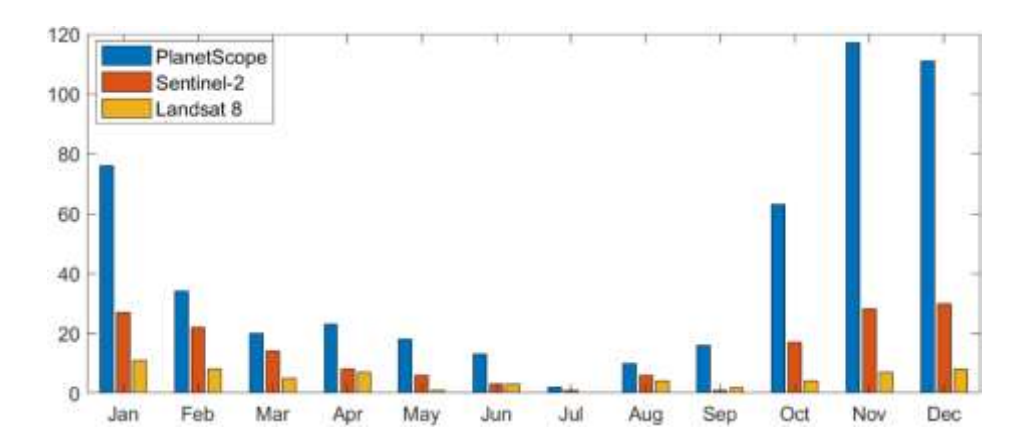
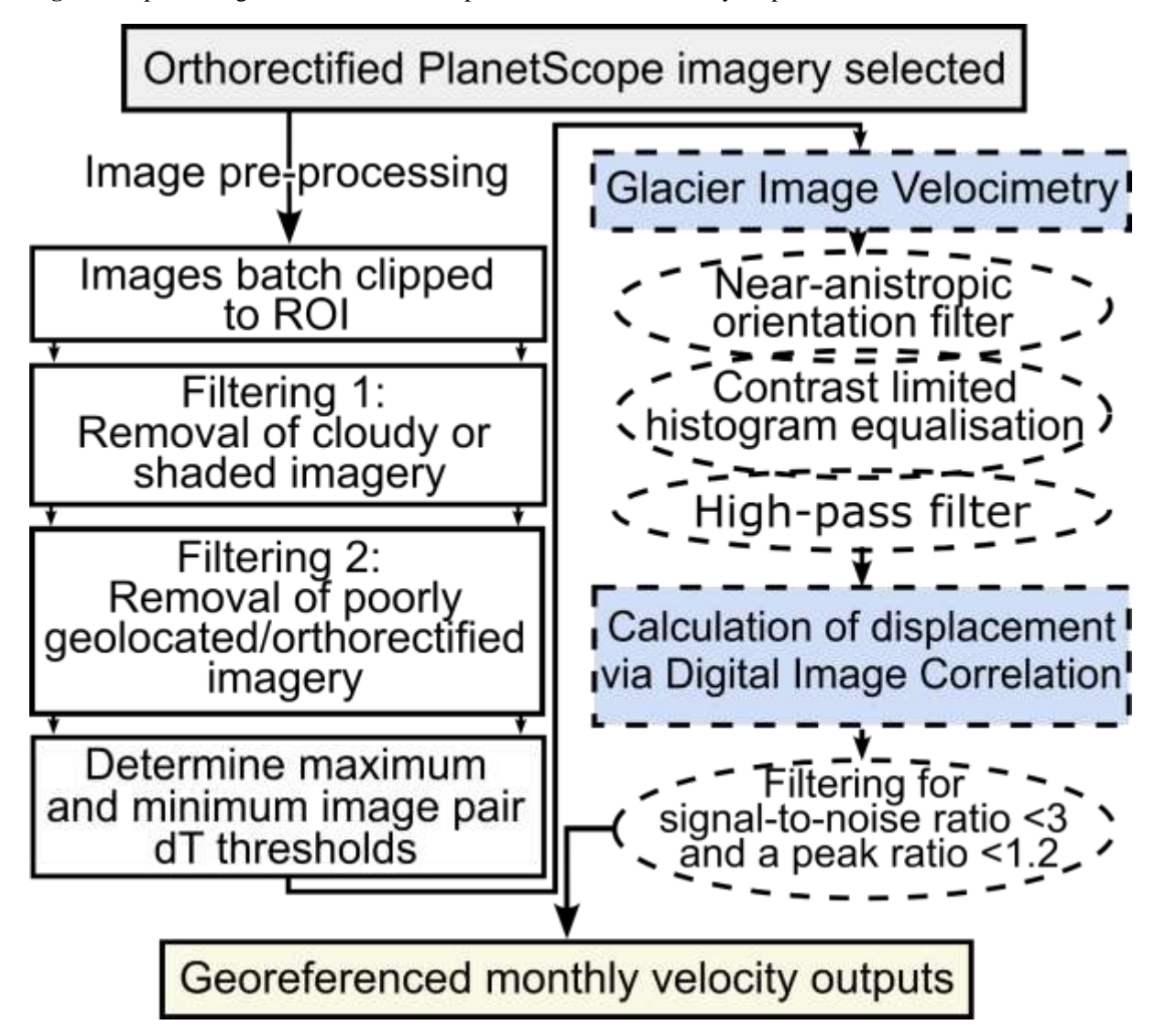
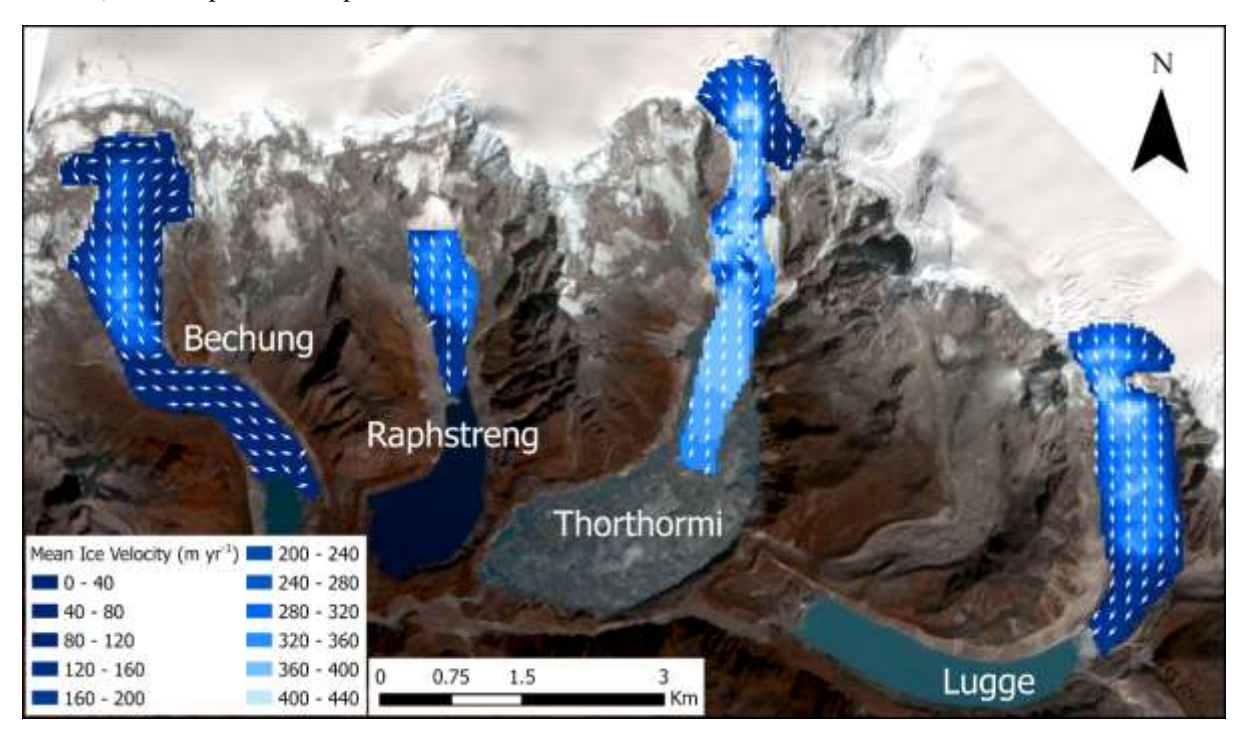


Fig. 3. The processing chain from PlanetScope Ortho Scenes to velocity outputs.



**Fig. 4.** Spatial distribution of mean ice velocities for the four study glaciers with average flow directions (2017 to 2023). Basemap; PlanetScope 2021.



**Fig. 5.** Mean monthly ice velocities for the study glaciers across the regions of interest (Red lower, blue upper); Bechung (a), Raphstreng (b), Thorthormi (c), Lugge (d). Stable ground uncertainty indicated in grey along the bottom.

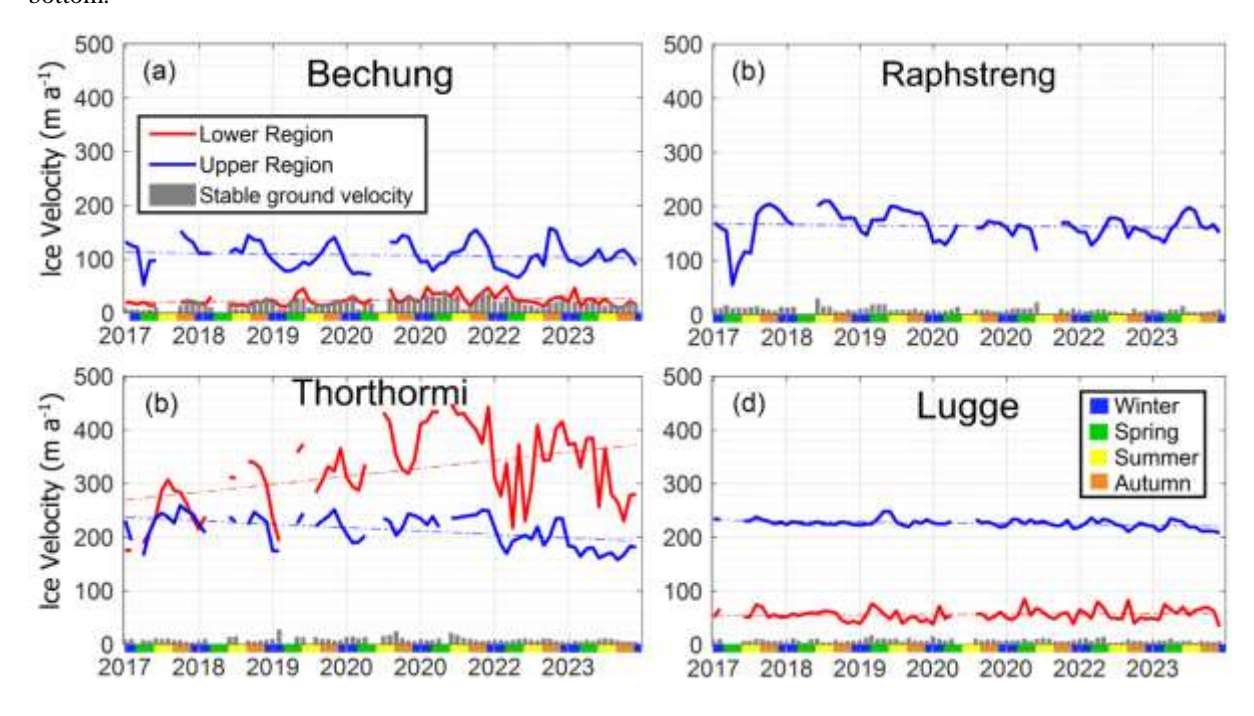


**Fig. 6.** Left: changes in average seasonal velocity from 2017 to 2023, for Bechung (a), Raphstreng (d), Thorthormi (f), Lugge (i). From figure left to centre follows changes from Winter to Spring, Spring to Summer, Summer to Autumn, Autumn to Winter. Right: average monthly ice velocities 2017 to 2023 for the lower and upper regions of Bechung (b-c), Raphstreng (e), Thorthormi (g-h), Lugge (j-k).

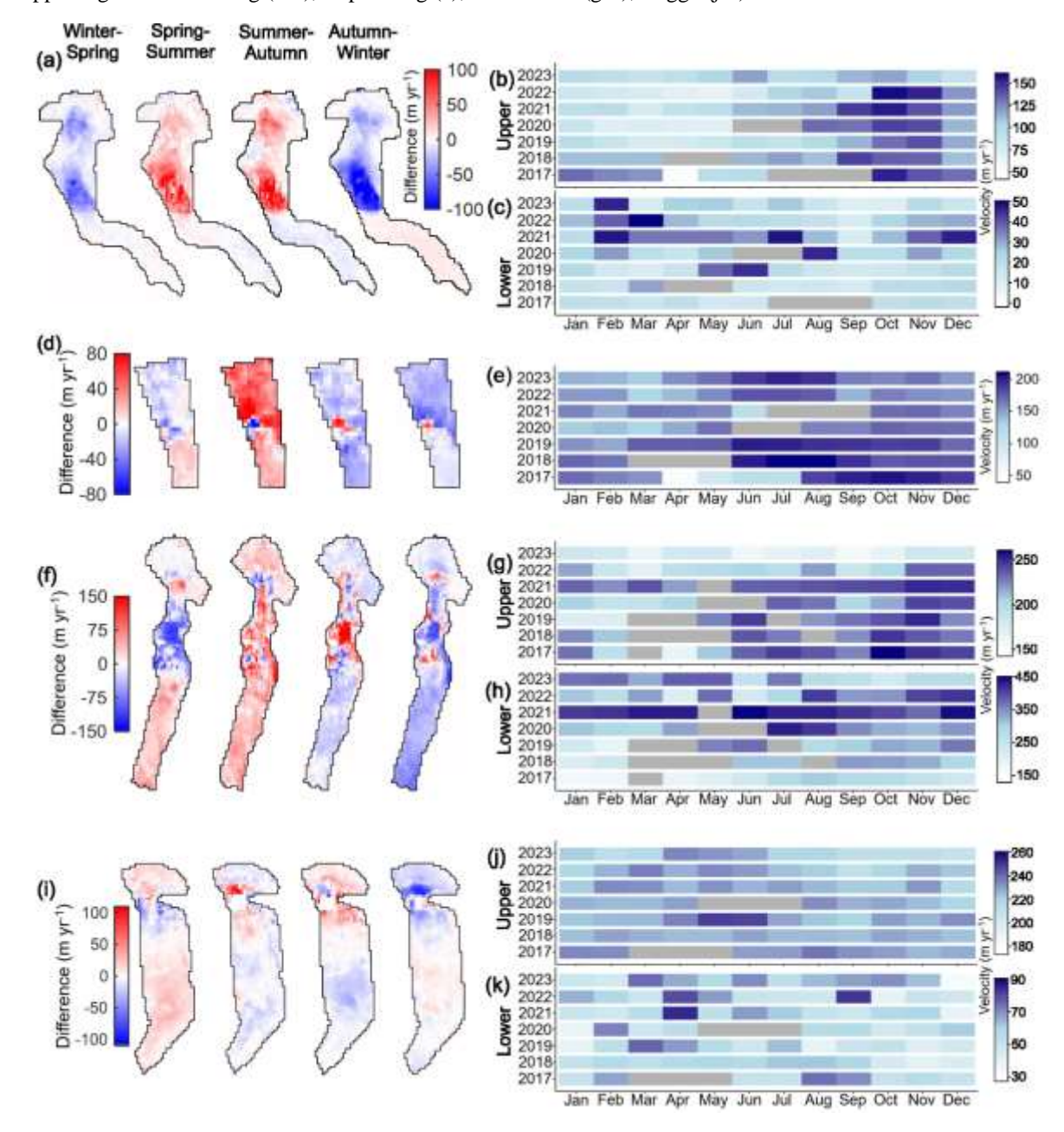
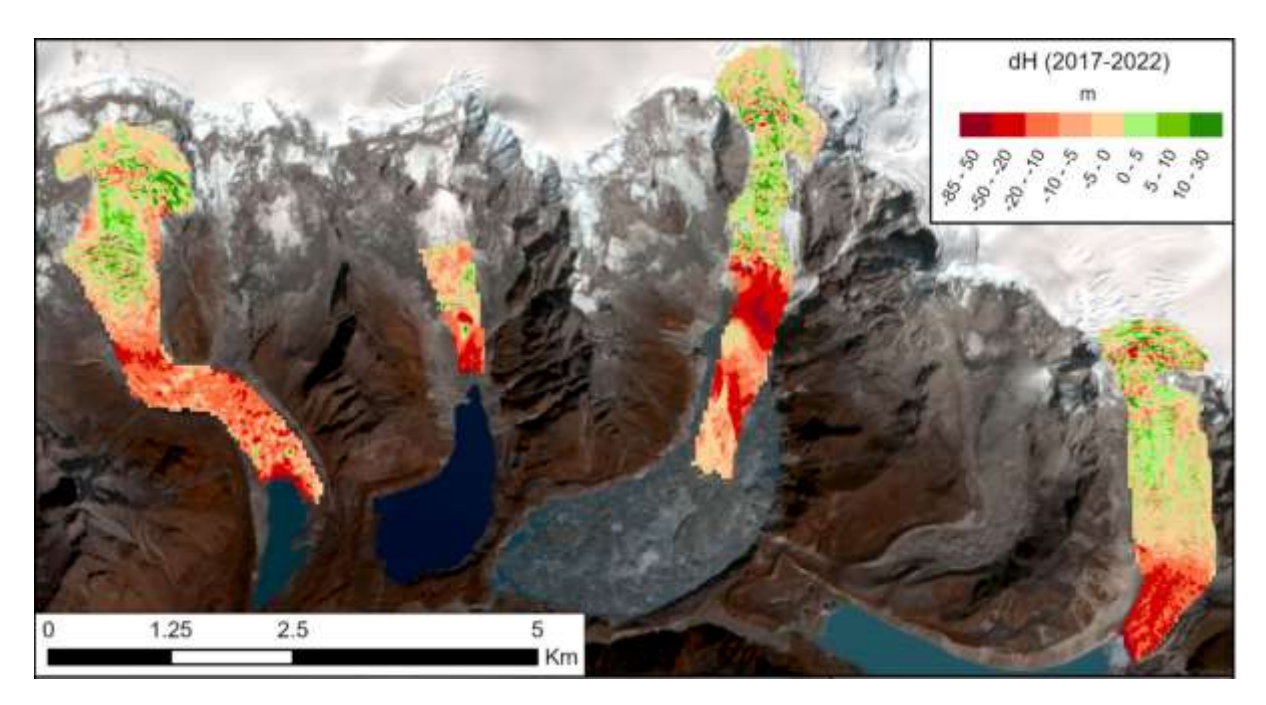
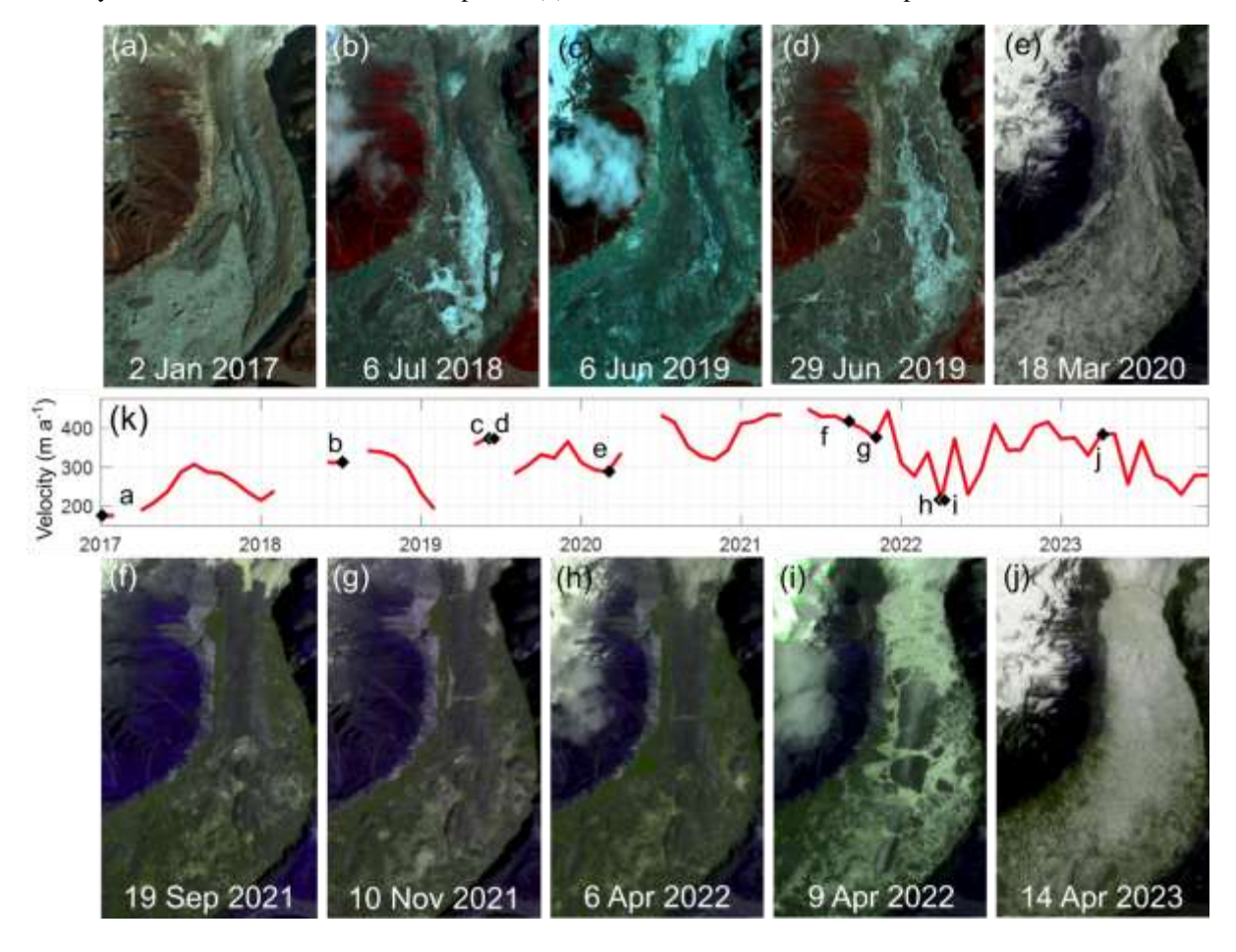


Fig. 7. Change in surface elevation (±1.03 m)(dH), between 2017 and 2022 for the four study glaciers



**Fig. 8.** Stages of the break-up of Thorthormi's terminus from 2017 to 2023 (a-j), compared with ice mean velocity across the terminus for the same period (k). The width of each scene corresponds to a scale of 2 km.



# **Tables**

**Table 1.** Summary of satellite capabilities used for observation in High Mountain Asia, including spatial resolution, sampling frequency, wavelength range and service durations.

Satellite type	Spatial	Sampling	Wavelength	Service	Example uses
	resolution	frequency	range	duration	
	(m)	(days)	(nm)		
PlanetScope Dove	3m	>1	443 – 565	2016-	(Millan and others, 2019;
(Planet, 2024)			(865 as of		Watson and others,
			2021)		2020)
Sentinel-2A/B	10 – 60	5	780–886	2015-	(Millan and others, 2019;
(ESA, 2023)					Pronk and others, 2021;
					Van Wyk de Vries and
					Wickert, 2021).
Sentinel-1A/B	20	6	(SAR)	2014-	(Gardner and others,
(ESA, 2023)					2018)
Landsat 8 (USGS,	30	15	500-680	2013-	(Gardner and others,
2023)					2018)
Landsat 7 (USGS,	15 – 60	15	520-900	1999-	(Dehecq and others,
2023)					2019; Agarwal and
					others, 2023)
SPOT 6 and 7	1.5 - 6	1-3	450-890	2012-	
(ESA, 2023)					
TerraSAR-X (ESA,	1 - 16	11	(SAR)	2007-	(Paul and others, 2022)
2023)					
Pléiades 1A and	0.5 - 2	26	430–830	2011-	(Ruiz and others, 2015;
1B (ESA, 2023)					Millan and others, 2019)

**Table 2.** Variable GIV input parameters for the four study glaciers. Maximum and minimum image separations and the defined oversampling range for each image pair.

Glacier	Maximum	Minimum	Maximum	Mean stable	Mean stable
	oversampling	Interval	Interval	ground velocities	ground velocities
	range (days)	(days)	(days)	(± m a <sup>-1</sup> )	(pixel units a <sup>-1</sup> )
Bechung	15	7	90	21.9	7.3
Raphstreng	15	7	90	10.4	3.5
Thorthormi	10	7	45	10.0	3.3
Lugge	10	7	90	8.5	2.8

**Table 3.** Surface area for the regions of interest across the four study glaciers, including the average slope for each region of interest. Thorthormi's lower region of interest is described for 2021 as the region area is frequently varied throughout the study given the rapid changes in spatial extent of the terminus over the study period.

Glacier	Surface area (km²)		Average slope ( <sup>0</sup> )	
	Lower	Upper	Lower	Upper
Bechung	0.79	1.21	17.9	27.9
Raphstreng	0.84		29.8	
Thorthormi (2021)	0.48	2.23	7.1	31.2
Lugge	0.51	1.17	16.8	28.2

**Table 4**. Rate of surface elevation change compared with previous studies for Thorthormi and Lugge. (Data up to the present study compiled by Sato and others (2022)).

Sampling period	Thorthormi rate of	Lugge rate c	of Study
	change (m a <sup>-1</sup> )	change (m a <sup>-1</sup> )	
1975 to 2000	-0.16	-1.20	Maurer and others (2019)
2000 to 2016	-1.30	-3.50	Maurer and others (2019)
2000 to 2016	-1.29	-3.81	Brun and others (2017)
2004 to 2011 (DGPS)	-1.40 ±0.27	-4.60 ±0.27	Tsutaki and others (2019)
2004 to 2011 (ASTER)	-1.61 ±2.75	-2.24 ±0.62	Tsutaki and others (2019)
2011 to 2018	-2.78 ±0.62	-2.87 ±0.62	Sato and others (2022)
2017 to 2022	-2.32 ±0.17	-4.00 ±0.17	This study